Quantitative analysis of electrically detected Ramsey fringes in P-doped Si

P. T. Greenland, G. Matmon, and B. J. Villis
London Centre for Nanotechnology and Department of Physics and Astronomy, University College London, London WC1H 0AH, United Kingdom

E. T. Bowyer, Juerong Li, and B. N. Murdin
Advanced Technology Institute and SEPNet, University of Surrey, Guildford, Surrey GU2 7XH, United Kingdom

A. F. G. van der Meer and B. Redlich
Radboud University, Institute for Molecules and Materials, FELIX Laboratory, Toernooiveld 7c, 6525 ED Nijmegen, The Netherlands

C. R. Pidgeon
Institute of Photonics and Quantum Science, SUPA, Heriot-Watt University, Edinburgh EH14 4AS, United Kingdom

G. Aeppli
Laboratory for Solid State Physics, ETH Zurich, Zurich, CH-8093, Switzerland;
Institut de la Matière Complexe, EPF Lausanne, Lausanne, CH-1015, Switzerland;
and Swiss Light Source, Paul Scherrer Institut, Villigen PSI, CH-5232, Switzerland

(Received 21 June 2015; revised manuscript received 10 September 2015; published 13 October 2015)

This work describes detection of the laser preparation and subsequent coherent manipulation of the quantum states of orbital levels of donors in doped Si, by measuring the voltage drop across an irradiated Si sample. This electrical signal, which arises from thermal ionization of excited orbital states, and which is detected on a millisecond time scale by a voltmeter, leads to much more sensitive detection than can be had using optical methods, but has not before been quantitatively described from first principles. We present here a unified theory which relates the voltage drop across the sample to the *wave function* of the excited donors, and compare its predictions to experiments in which pairs of picosecond pulses from the Dutch free-electron laser FELIX are used to resonantly and coherently excite P donors in Si. Although the voltage drop varies on a millisecond time scale we are able to measure Ramsey oscillation of the excitation on a picosecond time scale, thus confirming that the donor wave function, and not just its excited state population, is crucial in determining the electrical signal. We are also able to extract the recombination rate coefficient to the ground state of the donor as well as the photoionization cross section of the excited state and phonon induced thermal ionization rate from the excited state. These quantities, which were previously of limited interest, are here shown to be important in the description of electrical detection, which, in our unoptimized configuration, is sensitive enough to enable us to detect the excitation of $\sim 10^7$ donors.

DOI: 10.1103/PhysRevB.92.165310 PACS number(s): 42.50.Md, 78.47.jh, 78.47.jb, 78.47.da

I. INTRODUCTION

Previous experiments, using a free electron laser (FEL) source of coherent THz excitation, have shown that the orbital states of donors in Si can be manipulated in the same way as the orbital states of atoms or ions in traps [1,2]. However, phonon emission channels in Si lead to the rapid decay of excited states without a useful photon signal and this limits the number of excited donors which can be detected optically [3]. Very recently we have demonstrated the coherent creation and destruction, via Ramsey interference of picosecond pulse pairs, of orbital wave packets in Si:P with both optical and electrical read-out [4]. The electrical detection mechanism, termed photothermal ionization spectroscopy, is based on the much higher thermal ionization probability for an excited $2p_\pm$ state than the ground $1s$ state, implying that at finite temperature the sample conductivity directly reflects the strength of the $1s$ to $2p_\pm$ orbital transitions [4–7]. Electrical detection of orbital excitation is by orders of magnitude more sensitive than the optical technique (see also Refs. [8,9] for methods of electrical detection of *spin* resonances), enabling the detection of less than 10^5 electrons excited into the conduction band. It has the advantage that the sample is also the detector, enabling a unified theory of excitation and detection, which links the slow electrical response (millisecond) directly to the picosecond dynamics of the laser excitation. In the present work we present such a quantitative analysis of earlier experiments, where we measure the voltage response of a current-biased P-doped Si sample under irradiation by pairs of FEL laser pulses, tuned to the THz frequency of the $1s2p_\pm$ transitions. These pairs of pulses interact coherently to produce Ramsey interference fringes which we detect through variations in the sample conductance.

This two-pulse coherent excitation of a selected donor state is exactly the kind of manipulation envisaged in some quantum information processing schemes [10], so it is important for the modeling of such schemes to be sure that our understanding of the physics is complete. As we shall see below, the electron recombination rate from the conduction band, the photoionization cross section from the upper state, and the thermal ionization rate from the upper state are parameters important in the full description of the excitation process. Fortunately

we can extract these quantities from a comparison between theory and experiment, thus giving us a fully predictive model of the coherent manipulation of donors in Si by resonant laser excitation. To our knowledge, this is the first time that information has been obtained from both the absolute amplitude and the time dependence of coherent photoconductivity measurements.

In Sec. II we discuss the experiment and excitation dynamics of the donor electrons; in Sec. III we show, in detail, how the voltage drop across the sample is related to the population of the Si conduction band produced by the laser excitation, and how, by fitting the measured voltage drop as a function of time, we can extract not only the object of interest, the conduction band electron density, but also the free electron–ionized donor recombination coefficient and the effective circuit capacitance. In Sec. IV we compare the measured conduction band density as a function of laser interpulse separation with the result of theoretical predictions using a master equation, and find good agreement, thus confirming both the electrical and excitation models. These results, and what we learn from them, are discussed in Sec. V, and some conclusions are drawn in Sec. VI.

II. EXPERIMENT

All the experiments [11] are done as four-point, current-biased measurements with a phosphorus-doped silicon sample [12], doped at 2×10^{20} donors m^{-3} (see Fig. 1). Typically a constant current of 10 to 100 μA is passed between the outer terminals of the sample, and the voltage across the inner terminals under laser irradiation is recorded as a function of time on an oscilloscope. Our light source is the Dutch free-electron laser FELIX [13]. This produces trains of ∼100 transform-limited pulses with a duration of ∼5 ps, tuneable carrier frequency ∼9.5 THz, and interpulse interval of 40 ns. Each such train is called a macropulse, and each component of the train a micropulse. We use a beam splitter and delay stage to separate each micropulse in the train into a pulse pair with a separation of $t_d \sim$ ps. The macropulse energies of the two pulses in this pair, before final attenuation by the attenuator A_2 (see Fig. 1), are $E^{(1)} = 75$ μJ and $E^{(2)} = 44$ μJ, which are sufficiently similar for our purpose; the beams are focused to a waist of $r_0 = 1.9$ mm at the target. The final attenuations supplied by A_2 for the six experiments discussed here are shown in Table I.

The sample was mounted in vacuum on the cold finger of a continuous flow liquid helium cryostat, with polypropylene windows. The temperature, measured with a sensor on the heat exchanger at the top of the finger, was 9.5 K. We may calculate the maximum temperature rise due to FELIX irradiation as

$$\Delta T = \Delta J / C_s,$$

where ΔJ is the total energy absorbed by the sample over the course of a FELIX macropulse, and C_s is the sample specific heat [14]. If we assume that all the FELIX energy goes into heating the sample we find

$$\Delta T \sim 0.2 \text{ K}$$

for experiment 1, and correspondingly less for experiments 2 to 6. The thermal diffusion coefficient [15] for Si at 9.5 K is 0.69 m^2 s^{-1} so the thermal relaxation time is ∼μs.

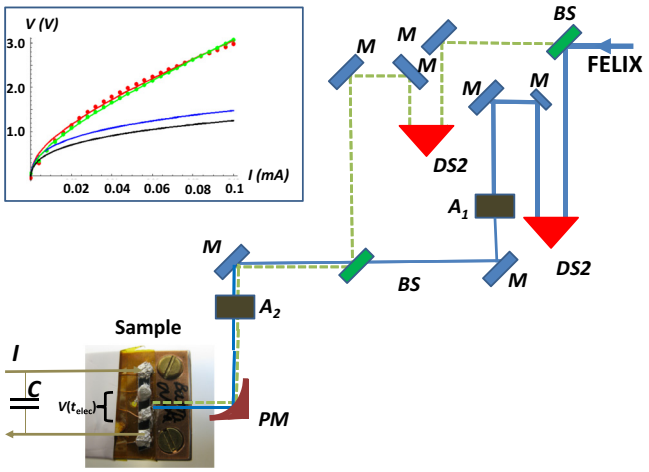

FIG. 1. (Color online) A schematic of the experiment. The FELIX beam enters at the top right and by a series of mirrors (M) and beam splitters (BS) is divided into two, sent through two delay lines (DS2) which control the pulse arrival times (t_d) and recombined, before being focused onto the sample with a parabolic mirror (PM). The FELIX polarization is perpendicular to the plane of the optical table. Attenuator A_1 is used to (approximately) equalize the beam intensities and A_2 controls the total intensity arriving at the target. The four-point current-biased configuration with current I and voltage drop $V(t_{elec})$ and circuit capacitance C is sketched. The sample I–V characteristic at 10 K is shown as an inset. The upper pair of lines and points are the total voltage drop [upper (red) data is forward bias, lower (green) data is reverse bias]. The lower pair of curves are the barrier voltage drop [upper (blue) curve is forward bias, lower (black) curve is revese bias]. The total measured voltage drop is shown as points; the solid lines show the I–V characteristics for a barrier voltage of $V_B = 1.3$ V, the value used in the analysis of the experiments. (See Ref. [12], Chap. 3). The I-V measurements were made at the London Centre for Nanotechnology on the same sample, and under the same conditions as the experiments described here.

Thus there is no thermal recovery between micropulses, but complete thermal recovery between macropulses. The change in temperature during a macropulse has a negligible effect on conductance.

In the absence of FELIX we expect, and find, that the voltage is constant. If we irradiate the sample with a sequence of FELIX pulses the voltage changes with time. It drops when the FELIX pulses arrive, and then recovers to its original value. The details of the voltage drop depend upon the separation of the pulse pair and the laser intensity. This is because the FELIX pulses increase the conduction band electron density, thereby increasing the sample conductance, and thus reducing the voltage, which then recovers as recombination occurs. Figure 2 shows the resonant excitation process we consider.

The time scale for the measured voltage behavior is set by the electrical properties of the circuit—essentially RC,

TABLE I. The final attenuations: A_2 is the actual attenuation, in dB, used in the experiment labeled by index k.

k	1	2	3	4	5	6
A_2	24.6	33.1	36.0	37.7	40.6	40.3

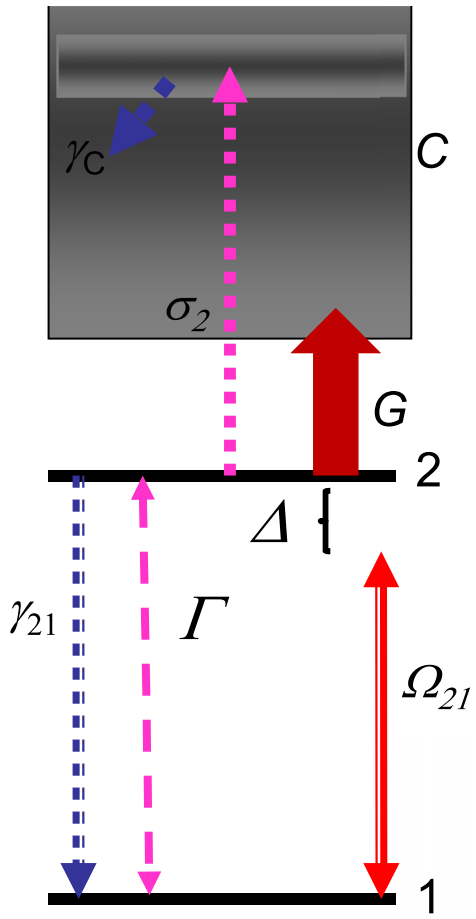

FIG. 2. (Color online) The excitation process: A FELIX pulse nominally resonant with the 1–2 transition, but with detuning Δ excites population into the upper level with instantaneous Rabi frequency Ω_{21}. After this pulse is over the donor is left in a linear combination of states 1 and 2 determined by the pulse area. A second pulse (not shown) further modifies the upper state population. The upper state can be thermally ionized into the conduction band at rate G, or photoionized at a rate determined by σ_2 the photoionization cross section from the upper level. Decay via phonon emission back to the ground state at the rate γ_{21} is a competing process. Dephasing processes at rate Γ are also included in the model.

where R is the circuit resistance, dominated by the sample resistance, and C is the circuit capacitance, which we assume is dominated by the wiring. Since the capacitance depends on the exact configuration of the leads, etc., we allow it to vary between experiments and determine it by fitting the voltage drop, as described below.

As described above, each FELIX micropulse is split into a pair with a beam splitter so that a FELIX macropulse will contain ~100 micropulse pairs. The separation between the pair of pulses is set to be t_d with $t_d \sim$ ps. Each pair is separated from its next neighbor by the micropulse repetition rate of 40 ns, and since the excited state lifetime of the donors $T_1 \sim 200$ ps we may assume that any *excitation* produced by a pair will have completely decayed before the next pair in the macropulse arrives. Furthermore, each macropulse lasts ~4 μs, much shorter than the characteristic voltage recovery time (100 μs), which in turn is much shorter than the 100 ms between macropulses, so we may assume complete relaxation of the sample between macropulses.

For each pulse pair separation, i.e., for each value of t_d, we record the voltage across the sample as a function of time. To avoid confusion with other time dependencies, we call the temporal parameter for these traces t_{elec}. Typically we record the traces for $t_{elec} \sim 300$ μs, very much longer than the times associated with the FELIX pulses.

Now we may calculate the sample resistance R_s at conduction band density n_e as [12]

$$R_s = \frac{L_s}{A_s e n_e \mu}, \tag{1}$$

where L_s is the sample length, A_s its cross sectional area, μ is the electron mobility, and e is the charge on the electron. If the sample carries current I_s, the total voltage across the sample is

$$V_s = V_B + I_s R_s, \tag{2}$$

where V_B is the barrier voltage, a function of I_s. Thus, knowing the I-V characteristic of the sample, and hence V_B, the sample dimensions, and the electron mobility at the sample temperature, we may derive the equilibrium electron density n_{eq} from V_s and I_s.

Now if we assume that this equilibrium density is maintained by some excitation process, with rate S, such as photoexcitation by black body radiation from the room temperature windows just above the sample, then the conduction band electron density n_e satisfies

$$\dot{n}_e = -P n_e (n_e + n_c) + S(n_P - n_e - n_c), \tag{3}$$

where n_P is the doping density, n_c is the compensation density, and P is the recombination rate coefficient. Noting that $\dot{n}_e = 0$ when $n_e = n_{eq}$, we can eliminate S and show that the conduction band density $n_e(t)$ as a function of time t is

$$n_e(t) = \frac{n_0 n_v e^{-t/\tau_c} + n_{eq}(n_T + n_0)}{n_0(1 - e^{-t/\tau_c}) + n_T}, \tag{4}$$

where n_0 is the *extra* electron density added to the conduction band at time $t = 0$ by the FELIX pulses [16]. Here

$$n_v = \frac{(n_c + n_{eq})(n_P - n_c)}{n_P - n_c - n_{eq}}$$

is, approximately, the number of recombination centres at equilibrium

$$n_T = n_{eq} + n_v \sim 2n_{eq} + n_c$$

and finally

$$\tau_c = 1/(n_T P)$$

is the characteristic recombination time [17]. Thus we can express the relaxation of the conduction band electron density to n_{eq} in terms of the recombination rate coefficient P, the equilibrium conduction band electron density n_{eq}, the compensation density n_c, and the dopant density n_P.

We now assume that a micropulse pair arriving at $t_{elec} = 0$ promotes n_1 electrons to the conduction band. We can use Eq. (4) to calculate the conduction band electron density at $t_{elec} + 40$ ns, when the next micropulse pair arrives and adds its contribution, to give a total extra density in the conduction

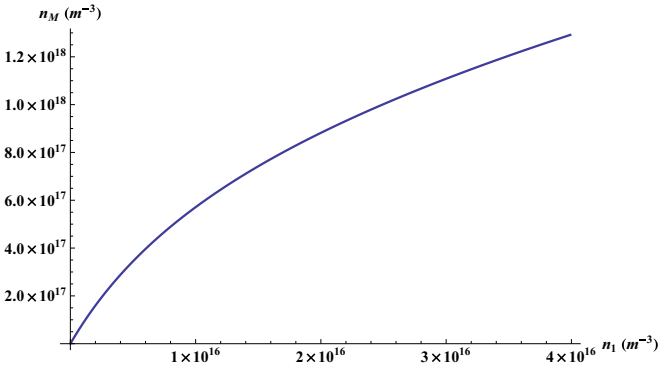

FIG. 3. (Color online) The effective multipulse ionization density n_M as a function of initial single pulse ionization density n_1, for $M = 100$ micropulses separated by 40 ns. We assume $n_{eq} = 3 \times 10^{16}$ m^{-3}, $n_c = 5 \times 10^{16}$ m^{-3}, and $P = 5.3 \times 10^{-13}$ m^3 s^{-1}, values typical of these experiments.

band. We can continue this process until all M micropulse pairs have passed and the conduction band density is n_M (see Fig. 3). On the time scale of the voltage change even the macropulse looks instantaneous, so the effect of a macropulse is to "instantaneously" promote n_M electrons to the conduction band ($n_0 = n_M$). Equation (4) can then be used to calculate the subsequent conduction band density and, therefore, through Eq. (1), the sample resistance as a function of time.

III. ELECTRICAL MATTERS

We know V_0, the equilibrium voltage at current I_s, and from Eqs. (1), (2), and (4) we have an analytic form for the sample resistance as a function of time. Remarkably, for the circuit shown in Fig. 1, we may solve the Kirchoff equations to obtain the voltage across the sample. It is

$$
\begin{aligned}
V(t) = {} & V_B + (V_0 - V_B) \\
& \times \Bigg(\Theta(t - t_p) \Bigg\{ \left[\frac{n_T + n_M}{n_T + n_M(1 - e^{-(t-t_p)/\tau_c})} \right]^{\frac{\tau_c n_T}{\tau_0 n_{eq}}} \\
& \times \Bigg[{}_2F_1\left(-\frac{\tau_c}{\tau_0}, -\frac{n_T \tau_c}{n_{eq}\tau_0}; 1 - \frac{\tau_c}{\tau_0}; \frac{e^{-\frac{t-t_p}{\tau_c}} n_M}{n_M + n_T} \right) \\
& - e^{-\frac{t-t_p}{\tau_0}} {}_2F_1\left(-\frac{\tau_c}{\tau_0}, -\frac{n_T \tau_c}{n_{eq}\tau_0}; 1 - \frac{\tau_c}{\tau_0}; \frac{n_M}{n_M + n_T} \right) \Bigg] \\
& + e^{-\frac{t-t_p}{\tau_0}} \left[\frac{n_T}{n_T + n_M(1 - e^{-(t-t_p)/\tau_c})} \right]^{\frac{\tau_c n_T}{\tau_0 n_{eq}}} \Bigg\} \\
& + \Theta(t_p - t) \Bigg),
\end{aligned}
\tag{5}
$$

where t_p is the time at which the conduction band density increases by n_M, and

$$\tau_0 = C L_s/(e\mu A_s n_{eq}) \quad (= C(V_s - V_B)/I_s),$$

where C is the circuit capacitance and $L_s/(e\mu A_s n_{eq})$ is the sample equilibrium resistance, so that τ_0 is the electrical time constant of the circuit. Here L_s is the effective sample length, A_s is the effective sample cross sectional, and μ is the electron mobility. We use $L_s = 2$ mm, $A_s = 1.6 \times 10^{-6}$ m^2, derived

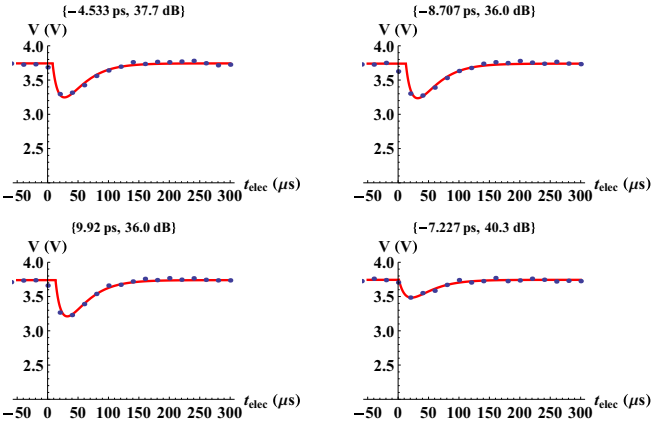

FIG. 4. (Color online) Four fits of the voltage drop chosen at random. The red line is the best fit voltage, the blue points are the measured values. Each graph is labeled by $\{t_d, A_2\}$, where t_d is the interpulse delay in picoseconds and A_2 is the total attenuation. An example of the corresponding conduction band density is shown in Fig. 5.

from the sample dimensions, and $\mu = 10$ m^2 V^{-1} s^{-1}, derived from a fit to literature values [18]. In Eq. (5) ${}_2F_1(a,b;c;z)$ is a hypergeometric function and $\Theta(t)$ is a Heaviside step function. We also use t as a general time variable; it is equivalent to t_{elec} in the experiments.

There are three unknowns in Eq. (5): the circuit capacitance C, the recombination coefficient P, and the conduction band density n_M. These can be obtained by fitting Eq. (5) to the experimental data—the voltage traces $V(t_{elec})$ for each pulse separation t_d. We expect the recombination coefficient P, and the circuit capacitance C to be independent of the laser pulse area [19] or pulse delay t_d, but the density of electrons excited to the continuum n_M to be a strong function of both these parameters.

We focus first on experiments 2 to 6. These were done at high attenuation and, as we shall see, in contrast to experiment 1, the voltage drops are reasonably small; saturation is not a problem and fitting Eq. (5) to the experimental voltage profiles is straightforward. In Fig. 4 we show typical fits of the voltage drop to Eq. (5), for experiments 2 to 6, whence we find [20]

$$P = (5.3 \pm 0.7) \times 10^{-13} \text{ m}^3 \text{ s}^{-1}$$

and

$$C = 1.24 \pm 0.14 \text{ nF}.$$

These values apply to all these experimental data. Of course we expect that the recombination rate coefficient should be a property of the sample, and thus independent of the experiment. The fact that the capacitance does not change between experiments is, presumably, because the wiring was undisturbed between experiments. The fits also give us the continuum electron density n_M produced by the train of FELIX pulse pairs as a function of the pair separation t_d for each experiment.

Thus, the use of Eqs. (4) and (5) has enabled us to extract the conduction band electron density as a function of the laser interpulse delay t_d and, as we can see in Fig. 5, this is a

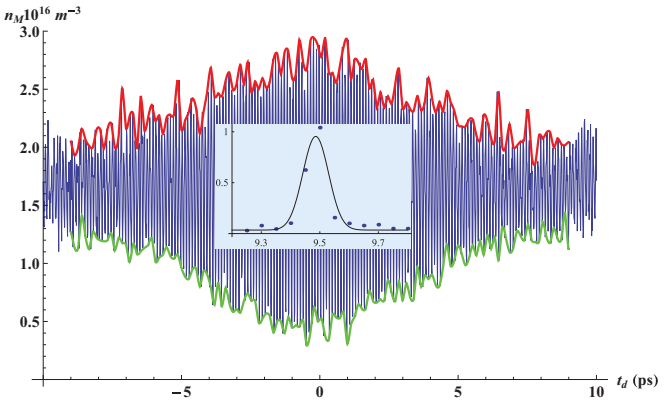

FIG. 5. (Color online) The conduction band density as a function of interpulse delay t_d for experiment 5. The actual experimental values are shown as a thin (blue) line. The upper border (shown in red) and the lower border (shown in green) are used in the fitting procedure described below. Also shown, as an inset, is the experimental power spectrum, normalized to unit height, as a function of frequency in THz (blue points), and in black, a Gaussian fit to it, showing that the rapid oscillations are indeed at the $1s$-$2p_\pm$ transition frequency of 9.49 THz.

strongly oscillating function of t_d, with a smooth envelope [21]. Our interest, however, is not the density in itself, but the coherent excitation of donor bound states by intense laser pulses [10,22]. As we have described in the Introduction, and illustrated in Fig. 2, we believe that the dominant mechanism for population of the conduction band is thermal ionization from the upper state excited by the FELIX pulses: this implies that the conduction band density is proportional to the upper state population produced by the laser excitation. Thus, the conduction band density serves as a measure of the excitation

TABLE II. The known data $|\boldsymbol{d}|$ is the radial matrix element for the ground state to $2p_\pm$ transition, T_1 and T_2 are the decay and dephasing times for this transition, G is the thermal photoionization rate from the $2p_\pm$ state, and $\tau_{\rm pulse}$ is the FELIX laser pulse duration.

$\lvert\boldsymbol{d}\rvert$ (nm)	T_1 (ps)	T_2 (ps)	G (s^{-1})	$\tau_{\rm pulse}$ (ps)
1.0	200	160	2.5×10^6	3.7

of the bound state by a FELIX pulse pair. All the processes shown in Fig. 2 can be included in a master equation [23]. If the solutions of this master equation reproduce the experimental results, we shall have confirmation that the electrical detection technique described here is capable of providing a useful alternative to the optical methods more usually used to detect coherent bound-state excitation.

From previous measurements using standard optical and electrically detected Fourier-transform infrared (FTIR) spectroscopy at different sample temperatures [24], we have good values for $|\boldsymbol{d}|$, the radial matrix element between the ground and excited donor states, and for G, the thermal ionization rate from the upper level. T_1 and T_2, the population and coherence decay rates, are known from pump-probe [2] and echo [1] experiments, and, of course $\tau_{\rm pulse}$, the laser pulse duration is obtained from standard pulse autocorrelation measurements. Thus, these parameters are known independent of the current experiments, and their values are shown in Table II.

IV. MODELING THE EXCITATION

Figure 2 shows all the important processes included in our model of the excitation process, which, of course, can be described by a master equation (in the rotating wave approximation [25])

$$\begin{pmatrix}\dot\rho_{11}\\ \dot\rho_{12}\\ \dot\rho_{21}\\ \dot\rho_{22}\end{pmatrix} = \begin{pmatrix} 0 & \frac{i\Omega_{21}(t)}{2} & -\frac{i\Omega_{12}(t)}{2} & \gamma_{21} \\ \frac{i\Omega_{12}(t)}{2} & -\frac{\gamma_{21}}{2}-\Gamma+i\Delta-\frac{F\sigma_2}{2}-\frac{G}{2} & 0 & -\frac{i\Omega_{12}(t)}{2} \\ -\frac{i\Omega_{21}(t)}{2} & 0 & -\frac{\gamma_{21}}{2}-\Gamma-i\Delta-\frac{F\sigma_2}{2}-\frac{G}{2} & \frac{i\Omega_{21}(t)}{2} \\ 0 & -\frac{i\Omega_{21}(t)}{2} & \frac{i\Omega_{12}(t)}{2} & -\gamma_{21}-F(t)\sigma_2-G \end{pmatrix}\begin{pmatrix}\rho_{11}\\ \rho_{12}\\ \rho_{21}\\ \rho_{22}\end{pmatrix}, \quad (6)$$

where $\boldsymbol{\rho}$ is the density matrix describing the state of a donor, and, as indicated in Fig. 2, the other parameters have the following meaning: $\Omega_{21}(t) = \Omega_{12}^*(t) = e\boldsymbol{d}\cdot\boldsymbol{E}(t)/\hbar$ is the instantaneous Rabi frequency produced by the laser pulses. Here $\boldsymbol{E}(t)$ is the instantaneous laser field envelope and $e\boldsymbol{d}$ is the transition dipole matrix element; Δ is the detuning between the laser carrier frequency and the donor transition frequency, γ_{21} is the population decay rate from level 2 to level 1, and Γ is the dephasing rate between levels 1 and 2 (i.e., $\gamma_{21} = 1/T_1$ and $\Gamma = 1/T_2$), σ_2 is the photoionization cross section from level 2, $F(t) = I(t)/\epsilon$ is the photon flux produced by the laser, where $I(t)$ is the instantaneous laser intensity and ϵ is the laser photon energy, and G is the thermal photoionization rate from the upper level. Of course $\Omega_{21}(t)$ and $F(t)$ are functions both of time and r, the radial distance from the beam axis, reflecting the two-pulse nature of the excitation and the Gaussian beam profile, respectively. Finally, we have

$$n_1(t,t_{\rm d}) = n_P\int_{-\infty}^{\infty} d\Delta g(\Delta)\int_0^R 2\pi r dr n_{\rm ion}(t,t_{\rm d},\Delta,r)/\mathcal{S}, \quad (7)$$

with

$$n_{\rm ion}(t,t_{\rm d},\Delta,r) = [1-\rho_{11}(t,t_{\rm d},\Delta,r)-\rho_{22}(t,t_{\rm d},\Delta,r)],$$

where $g(\Delta)$ is the inhomogeneous broadening profile, R (= 1 mm) is the radius of the illuminated region, set by an aperture in front of the sample, and $\mathcal{S}\sim\pi R^2$ is the effective area occupied by the conduction band electrons.

Thus, as Eq. (6) shows, in addition to the parameters in Table II we need to know the inhomogeneous broadening of the sample $g(\Delta)$ and the photoionization cross section from the upper level σ_2. We consider two inhomogeneous profiles,

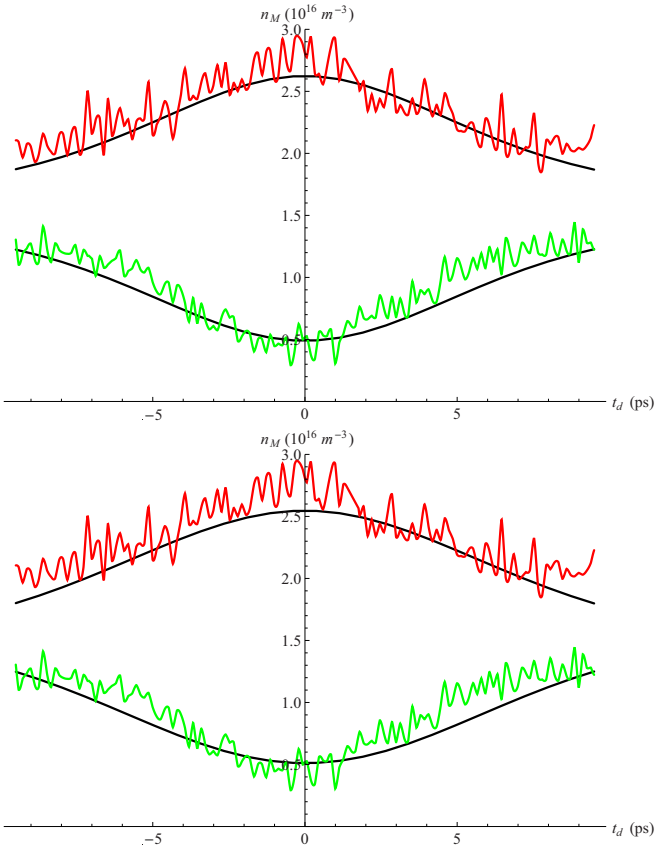

FIG. 6. (Color online) The fits to the experimental Ramsey fringe profiles for experiment 5, assuming a Lorentzian inhomogeneous profile (top) or a Gaussian inhomogeneous profile (bottom). As in Fig. 5 the upper and lower borders of the experimental continuum electron density as a function of interpulse delay are shown. The smooth black lines are the corresponding theoretical result. Fits to experiments 2, 4 and 6 are comperable; the fit to experiment 3 is slightly poorer. See text, and Table III for further details.

a Gaussian

$$g(\Delta) = \exp\left[-(\Delta - \Delta_0)^2/W_G^2\right]/\sqrt{\pi}W_G$$

and a Lorentzian

$$g(\Delta) = W_L/2\pi\left/\left[(\Delta - \Delta_0)^2 + W_L^2/4\right]\right..$$

Finally, there are two purely experimental features which we must take into account. First, absolute intensity measurements in this wavelength region are very uncertain, and in our setup it is difficult to know how much transmission loss we have between the target and the point in front of the polypropylene cryostat window where the beam intensity was measured, with a commercial portable pyroelectric power meter. We account for this by introducing $T_{\rm eff}$, defined so that

$$\boldsymbol{E}_{\rm target} = T_{\rm eff}\boldsymbol{E}_{\rm meas},$$

where $\boldsymbol{E}_{\rm meas}$ is the laser envelope field derived from the measured laser power, and $\boldsymbol{E}_{\rm target}$ is the laser field at the surface of the Si target. Previous experience [1] suggests that $T_{\rm eff} \sim 0.7$. Second, the FELIX radiation has a small

TABLE III. The fitting parameters. f is the percentage of third harmonic energy in the FELIX pulse, $T_{\rm eff}$ is the effective (electric field) transmission coefficient into the cryostat, W is the full width half maximum (FWHM) value of the inhomogeneous broadening, and σ_2 is the photoionization cross section from the upper level. L assumes a Lorentzian and G a Gaussian shape for the inhomogeneous broadening. The Lorentzian fit is marginally better.

Fit	f (%)	$T_{\rm eff}$	W (THz)	σ_2 (10^{-20} m^2)
L	2.3 ± 0.8	0.95 ± 0.1	0.057 ± 0.01	2.5 ± 1
G	2.5 ± 0.8	0.83 ± 0.08	0.073 ± 0.01	2.6 ± 0.4

third harmonic component [26]. Although this is at the few percent level it is important in these experiments because third harmonic photons are sufficiently energetic to ionize ground state donors directly. Since direct ionization does not show Ramsey fringes, its effect is to add a $t_{\rm d}$ independent background to the results calculated from Eq. (6). This background is of magnitude

$$n_x \sim f n_P \mathcal{A}\sigma_{1s}(3\epsilon_{2p_\pm})\frac{\mathcal{E}_{\rm in}\left[1 - {\rm e}^{-R^2/r_0^2}\right]}{3\pi r_0^2 \epsilon_{2p_\pm}}, \qquad (8)$$

where f is the fraction of the third harmonic, $\epsilon_{2p_\pm}$ is the transition energy, $\sigma_{1s}(3\epsilon_{2p_\pm})$ is the $1s_A$ ionization cross section at the third harmonic energy ($\sim 3 \times 10^{-20}$ m^2 from hydrogenic scaling), $\mathcal{A}$ is the beam attenuation, and $\mathcal{E}_{\rm in}$ is the total beam energy at the target.

The important physical content of the conduction band density is the envelope of the rapidly oscillating signal. We make a fit of the theoretical expression derived from Eqs. (7) and (8) to the results from experiments 2 to 6 simultaneously using the beam transmission $T_{\rm eff}$, inhomogeneous width W_L or W_G, cross section σ_2, and third harmonic component f as fitting parameters. A typical result is shown in Fig. 6, and the parameters given in Table III. The errors reflect the spread of values over the individual experiments. The fits themselves show errors of $\sim$13% per point, averaged over experiments 2 to 6. Nominally the error in the Lorentzian fit is smaller—13.1% compared with 13.3%—but this difference is, of course, not significant. Finally, we may remark that we have checked that both the fits to the voltage drops and the fits to the fringe envelopes are robust against variations in their starting parameters.

V. DISCUSSION

Electrically detected FTIR spectroscopy has been performed on our sample, and both Lorentzian and Gaussian fits made to the $2p_\pm$ line. It is found that the Lorentzian shape gives a systematically better fit [27]. The results are that, for a Lorentzian fit, the full width half maximum is

$$W_{\rm L}^{\rm FTIR} = 0.041 \pm 0.007\ {\rm THz},$$

and for a Gaussian fit, the FWHM is

$$W_{\rm G}^{\rm FTIR} = 0.047 \pm 0.01\ {\rm THz}.$$

Thus the values for the widths given in Table III are in broad agreement with the FTIR measurements, particularly as the

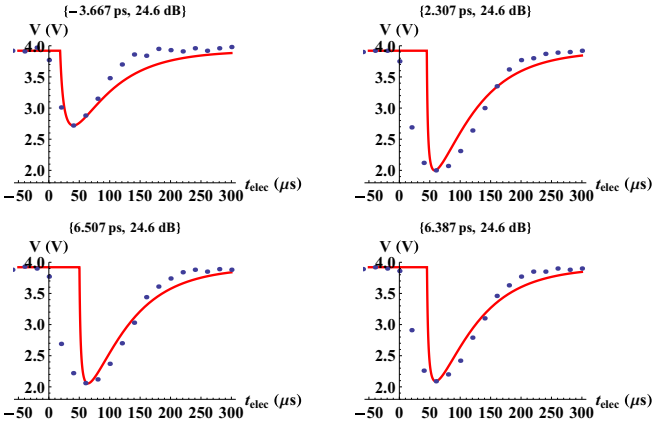

FIG. 7. (Color online) The analog of Fig. 4 for experiment 1. Here the voltage drop is typically much larger than in the previous cases.

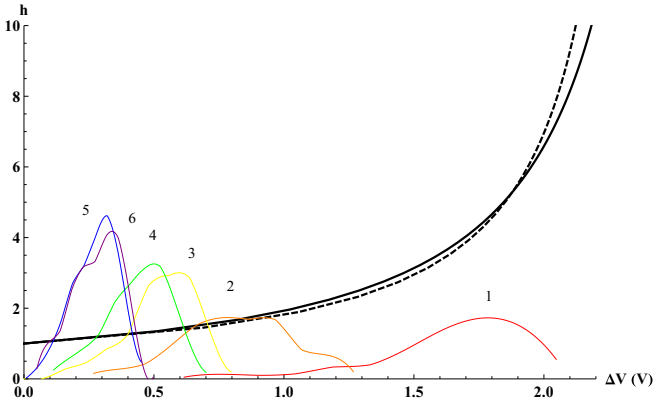

FIG. 8. (Color online) h, the ratio of the relative change in continuum electron density to the relative change in the corresponding maximum voltage drop ΔV, plotted as a function of ΔV for the parameters appropriate to experiment 1 (solid black line) and experiments 2 to 6 (dashed black line). Also shown are the experimental probability distributions for ΔV for the six experiments, each labeled with its experimental index. They have been scaled so that the vertical axis is correct for both h and the probability distributions.

linewidth is sensitive to strain induced by the sample mounting method. However, the agreement between the widths derived from the Ramsey fringe experiments and the FTIR spectra is better for the Lorentzian line shape than for the Gaussian. Once again, the difference is not conclusive (a 1.3 standard deviation difference for the Lorenzian shape as opposed to a 1.8 standard deviation difference for the Gaussian) but, as before, the Lorentzian shape is preferred. The photoionization cross section from the upper state has a large error but is consistent with the value expected from hydrogenic scaling. Furthermore, $T_{\rm eff}$ appears to be well determined by the fits, and suggests that 70%–90% of the measured input power is transferred to the surface of the sample. The value of f, the fraction of total energy in the third harmonic, is also at the level expected.

We now consider experiment 1. In Fig. 7 we show the analog of Fig. 4 for experiment 1, the fits of the voltage response as a function of $t_{\rm elec}$. The circuit capacitance obtained from these fits, the value which minimizes the maximum error over the set of voltage drops is

$$C_1 = 2.6\ \text{nF}.$$

Notice first that the fits are somewhat poorer, but, more important, because of the more intense excitation, and consequent increase in conduction band occupancy, the sample resistance is lower and thus, from Eq. (2), the total voltage drop is larger than in the other experiments. Now Eq. (2) also shows that the voltage drop must saturate—it can be no larger than $V_0 - V_B$. This has an important consequence that we can deduce from Eq. (5). For a given set of parameters $n_{\rm M}$, τ_0, τ_C, etc., we may calculate $\Delta V = V_0 - V_{\rm min}$, where $V_{\rm min}$ is the minimum voltage attained for the chosen set of parameters, i.e., ΔV is the maximum voltage drop attained for these parameters. We assume τ_0, τ_C, etc., are fixed, and focus on the behavior as a function of $n_{\rm M}$. We then have

$$\Delta V = F(n_{\rm M}),$$

where F is a function which could be derived from Eq. (5). We may invert this equation and, taking $G = F^{-1}$, derive

$$\frac{\delta n_{\rm M}}{n_{\rm M}} = h(\Delta V)\frac{\delta \Delta V}{\Delta V}, \tag{9}$$

with

$$h(\Delta V) = \Delta V G'(\Delta V)/G(\Delta V) \tag{10}$$

(of course h depends upon τ_0, τ_C, etc., as well). We may interpret Eq. (9) as meaning that the relative uncertainty in the continuum electron density $\delta n_{\rm M}/n_{\rm M}$ is proportional to the relative uncertainty in the maximum voltage drop $\delta\Delta V/\Delta V$ with the constant of proportionality given by $h(\Delta V)$. Now, for each experiment we have ∼1500 values of ΔV, one for each $t_{\rm d}$ from which we may construct a probability density function

$$P_k(\Delta V)d\Delta V, \tag{11}$$

which shows the distribution [28] of maximum voltage drops for experiment k. Thus, P_k defines the range over which ΔV varies for experiment k and $h(\Delta V)$ shows how errors in ΔV are propagated into $n_{\rm M}$. We show both $h(\Delta V)$ and $P_k(\Delta V)$ in Fig. 8. The implication of this figure is that even if the experimental errors in $V(t_{\rm elec})$ are the same for all the experiments, nevertheless the uncertainty in extracting the continuum electron density $n_{\rm M}$ from the behavior of $V(t_{\rm elec})$ grows with increasing maximum voltage drop, i.e., with increasing laser intensity.

In Fig. 9 we compare the experimental continuum density envelope with the theoretical prediction. Since these experimental results were not used in obtaining the quantities needed by theory (see Table III), this continuum density envelope is a true prediction. It agrees with experiment less well than in the other cases: we attribute this to the difficulty of extracting the continuum electron densities adumbrated above. Nevertheless, we believe the agreement is acceptable.

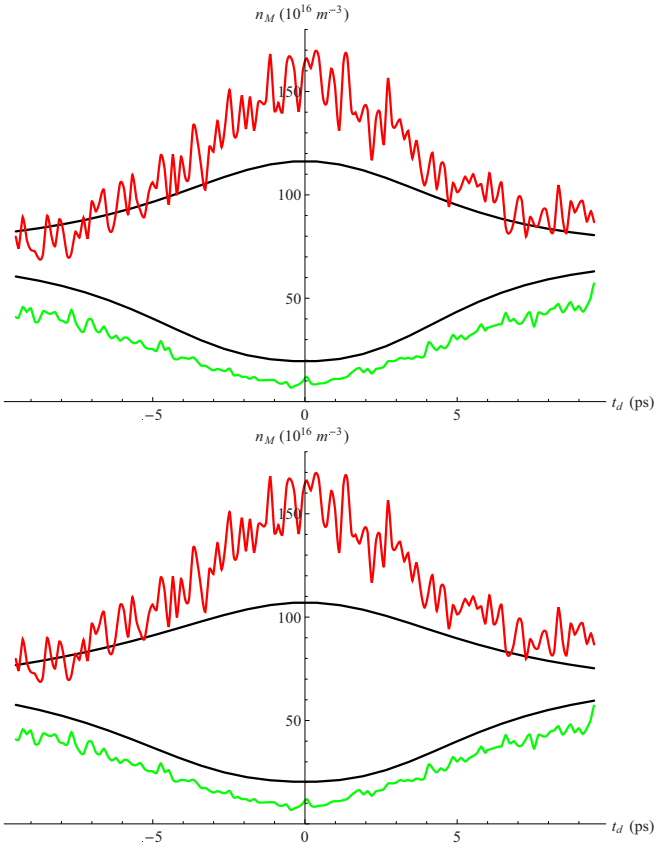

FIG. 9. (Color online) The analog of Fig. 6 for experiment 1. Notice that the agreement between theory and experiment is poorest at large n_M, where this is least well determined by the measured voltage drop (see Fig. 8).

VI. CONCLUSIONS

In summary, we have developed a theory of the coherent excitation of donors in Si and applied it to a description of the electrical detection of the coherent response of P donors to irradiation by pairs of THz laser pulses. Electrical detection is sensitive. Typically, in these experiments we detect the ionization of about one donor in 10^4, within a volume of $\sim 3 \times 10^{-9}$ m^{-3} implying a total of $\sim 10^7$ excited electrons, and, as Fig. 6 shows, the limit is certainly an order of magnitude better than this. However, as the analysis presented above shows, the small number of conduction band electrons is a result of the low thermal ionization rate of the excited state, a condition exacerbated by the use of lower operating temperatures. To exploit the method fully, direct readout methods which selectively ionize the excited state at low temperatures (where the photothermal channel is shut down), for example by using a long-wavelength intense laser, will have to be developed. These methods will then be suitable for dilute samples, where the saturation shown in Fig. 8 is not a problem.

However, what is more important is that in this study we have identified all the important physical processes which must be included in a theory of the coherent excitation of donors in Si. Many of these are the result of the solid-state environment of the donors, and would be absent in a trapped ion or atom. Nevertheless, their inclusion in the master equation that describes the excitation is straightforward, so that essentially the same techniques used in the description of the coherent control of ions and atoms in traps can be applied to donors in Si, once again suggesting that Si provides a "vacuumlike" environment for donors [1,2].

However, the analogy is not perfect. A major difference is that electrical detection, as used here, is sensitive to recombination, thus focusing attention on the effective recombination rate coefficient P. Here we find

$$P = 5.3 \times 10^{-13}\ \mathrm{m}^3\,\mathrm{s}^{-1},$$

which is close to

$$P_{\mathrm{BR}} = 2 \times 10^{-13}\ \mathrm{m}^3\,\mathrm{s}^{-1},$$

the value estimated from the Brown and Rodreguez [20] value of recombination cross section. However, Norton *et al.* [29] give the much larger value of

$$P_{\mathrm{N}} = 2.5 \times 10^{-11}\ \mathrm{m}^3\,\mathrm{s}^{-1}$$

close to the value

$$P_{\mathrm{B}} = 1.3 \times 10^{-11}\ \mathrm{m}^3\,\mathrm{s}^{-1}$$

found by Bowyer *et al.* [7]. It should be noted that the sample used here is similar to those considered by Brown and Rodriguez and Norton *et al.*, but very different from the metal oxide semiconductor field effect transistor (MOSFET) used by Bowyer *et al.* Recombination is a complex cascade process and the effective recombination rate coefficient will depend at least on temperature, donor density, trap density (which will vary strongly between bulk silicon and MOSFETs), and sample phonon spectrum, so the difference between our value and that in Ref. [7] is not surprising.

In summary, the important conclusion is that techniques which have been successfully applied to the modeling of quantum information processing in trapped ions and atoms [30] can, with little modification, also be used to model similar processes in donors in Si.

ACKNOWLEDGMENTS

We have enjoyed useful conversations with A. J. Fisher of University College London. We gratefully acknowledge the support of the EPSRC UK (COMPASSS, Grant Reference EP/H026622) and the FELIX facility Nijmegen Holland.

[1] P. T. Greenland, S. A. Lynch, A. van der Meer, B. N. Murdin, C. R. Pidgeon, B. Redlich, N. Q. Vinh, and G. Aeppli, Nature (London) **465**, 1057 (2010).

[2] N. Q. Vinh, P. T. Greenland, K. Litvinenko, B. Redlich, A. F. G. van der Meer, S. A. Lynch, M. Warner, A. M. Stoneham, G. Aeppli, D. J. Paul, C. R. Pidgeon, and B. N. Murdin, PNAS **105**, 10649 (2008).

[3] V. V. Tsyplenkov, E. V. Demidov, K. A. Kovalevsky, and V. N. Shastin, Semiconductors **42**, 1016 (2008).

[4] K. Litvinenko, E. Bowyer, P. Greenland, N. Stavrias, J. Li, R. Gwilliam, B. Villis, G. Matmon, M. Pang, B. Redlich, A. van der Meer, C. Pidgeon, G. Aeppli, and B. Murdin, Nat. Commun. **6**, 6549 (2015).

[5] A. K. Ramdas and S. Rodriguez, Rep. Prog. Phys. **44**, 1297 (1981).

[6] P. C. M. Planken, P. C. van Son, J. N. Hovenier, T. O. Klaassen, W. T. Wenckebach, B. N. Murdin, and G. M. H. Knippels, Phys. Rev. B **51**, 9643 (1995).

[7] E. T. Bowyer, B. J. Villis, J. Li, K. L. Litvinenko, B. N. Murdin, M. Erfani, G. Matmon, G. Aeppli, J.-M. Ortega, R. Prazeres, L. Dong, and X. Yu, Appl. Phys. Lett. **105**, 021107 (2014).

[8] R. N. Ghosh and R. H. Silsbee, Phys. Rev. B **46**, 12508 (1992).

[9] D. R. McCamey, C. Boehme, G. W. Morley, and J. van Tol, Phys. Rev. B **85**, 073201 (2012).

[10] A. M. Stoneham, A. J. Fisher, and P. T. Greenland, J. Phys. Condens. Matter **15**, L447 (2003).

[11] https://zenodo.org with DOI:10.5281/zenodo.30978.

[12] S. M. Sze and K. K. Ng, *Physics of Semiconductor Devices* (John Wiley and Sons, Hoboken, NJ, 2007).

[13] G. M. H. Knippels, X. Yan, A. M. MacLeod, W. A. Gillespie, M. Yasumoto, D. Oepts, and A. F. G. van der Meer, Phys. Rev. Lett. **83**, 1578 (1999).

[14] P. Flubacher, A. J. Leadbetter, and J. A. Morrison, Philos. Mag. **4**, 273 (1959).

[15] C. J. Glassbrenner and G. A. Slack, Phys. Rev. **134**, A1058 (1964).

[16] So that the *total* conduction band density at $t = 0$ is $n_0 + n_{\rm eq}$.

[17] The additional $n_{\rm eq}$ in the expression for $n_{\rm T}$ and τ_c comes from the circumstance that not only are there $n_{\rm v}$ recombination centers for a test electron in the continuum, but there are also $n_{\rm eq}$ additional electrons in the conduction band.

[18] C. Canali, C. Jacoboni, F. Nava, G. Ottaviani, and A. A. Quaranta, Phys. Rev. B **12**, 2265 (1975).

[19] A pulsed laser which produces an instantaneous Rabi freqency $\Omega(t) = e\boldsymbol{d} \cdot \boldsymbol{E}(t)/\hbar$, where $\boldsymbol{E}(t)$ is the laser's electric field envelope and $e\boldsymbol{d}$ is the dipole moment for the transition has a pulse area given by $\mathcal{A} = \int \Omega(t)dt$.

[20] R. A. Brown and S. Rodriguez, Phys. Rev. **153**, 890 (1967).

[21] We calculate the borders by partitioning the data into K contiguous regions each of length q. We then calculate $n_M^{\rm max}(k)$, $n_M^{\rm min}(k)$, the maximum and minimum value of the electron density in the kth region, and $t_{\rm d}(k)$, the mean value of the delay in the kth region. We take $B^{\rm max} = \{\bar{t}_{\rm d}(k), n_M^{\rm max}(k)\}, k = 1, \ldots, K$, to define the upper border and $B^{\rm min} = \{\bar{t}_{\rm d}(k), n_M^{\rm min}(k)\}, k = 1, \ldots, K$, to define the lower border. Too small a value of q gives a rapidly varying envelope, too large a value gives a slowly varying envelope that accentuates the maxima. Values of q between 7 and 15 give broadly similar results; we use $q = 10$, and interpolate $B^{\rm max}$ and $B^{\rm min}$ in the illustrations.

[22] F. A. Zwanenburg, A. S. Dzurak, A. Morello, M. Y. Simmons, L. C. L. Hollenberg, C. L. Lloyd, G. Klimeck, S. Rogge, S. N. Coppersmith, and M. A. Eriksson, Rev. Mod. Phys. **85**, 961 (2013).

[23] G. S. Agarwal, Phys. Rev. A **18**, 1490 (1978).

[24] B. J. Villis, G. Matmon, P. T. Greenland, D. Li, M. Erfani, X. Yu, B. N. Murdin, A. J. Fisher, and G. Aeppli (to be published).

[25] M. Fox, *Quantum Optics: An Introduction* (Oxford University Press, Oxford, 2006).

[26] Z. Huang and K.-J. Kim, Phys. Rev. E **62**, 7295 (2000).

[27] See Supplemental Material at http://link.aps.org/supplemental/10.1103/PhysRevB.92.165310 for details of these spectra and fits.

[28] Notice we have $\int_0^{V_0} P_k(\Delta V)d\Delta V = 1$; P_k itself can exceed 1.

[29] P. Norton, T. Braggins, and H. Levinstein, Phys. Rev. Lett. **30**, 489 (1972).

[30] F. Rohde and J. Eschner, in *Untracold Gases and Quantum Information*, Lecture Notes of Les Houches Summer School in Singapore, Vol. 91 (Oxford University Press, Oxford, UK, 2011).